EXTENSION FRACTURES, SECONDARY FAULTS AND SEGMENT LINKAGE IN STRIKE-SLIP FAULT SYSTEMS AT RAME HEAD, SOUTHERN CORNWALL

Y.-S. KIM[1], J.R. ANDREWS[1] AND D.J. SANDERSON[2]

KIM, Y.-S. ANDREWS, J.R. AND SANDERSON D.J. 2001. Extension fractures, secondary faults and segment linkage in strike-slip fault systems at Rame Head, Southern Cornwall. *Geoscience in South-West England*, **10**, 000-000.

At Rame Head, NW trending right-lateral strike-slip faults intersect nearly vertical E trending Lower Devonian beds. Faults are metres to several tens of metres long, with displacements from 0.1 - 5 m. They are accompanied by subsidiary left-lateral conjugate faults.

Propagation of the faults has left a wake of damage structures in the fault walls. Damage structures at Mode II fault tips are dominated by extensional horsetail splay fractures that were complicated by subsequent fault propagation and linkage. At wall zones, antithetic high angle fractures to the faults (R' or X) are the predominant fracture patterns.

Displacement-distance profiles show very variable and irregular shapes, mainly caused by segment linkage. The faults show significant displacements which have lead to the development of nested isolated lenses (strike-slip duplexes). Displacement rapidly decreases towards these structures with maximum displacements commonly located either side of the lenses, suggesting that they evolved from linkage of originally isolated fault tips or relay zones. Maximum displacement / fault length (d_{max}/L) plots show step-like growth paths compatible with segmented fault systems.

[1]School of Ocean and Earth Science, University of Southampton, Southampton Oceanography Centre, Southampton, SO14 3ZH, U.K. (E-mail jra2@soc.soton.ac.uk).
[2]TH Huxley School of Environment, Earth Sciences and Engineering, Imperial College, London, SW7 2BP, U.K.

INTRODUCTION

Numerous recent studies from a variety of tectonic settings have presented slip distribution data on faults and suggested the effects of fault geometry, segmentation and interaction on the shape of displacement profiles (e.g. Peacock, 1991; Bürgmann *et al*., 1994; Cartwright *et al*., 1995; Nicol *et al*., 1996; Willemse *et al*., 1996; Peacock and Sanderson, 1996; Fossen and Hesthammer, 1997; Cartwright and Mansfield, 1998). A common feature is that irregular distributions of displacement have been attributed to fault segmentation and linkage generally marked by either intact or linked relay structures. This paper addresses the question of how fault segmentation in strike-slip fault systems affects displacement-distance profiles where significant fault linkage has taken place.

Terminology

Isolated faults consist of elliptical surfaces which show a pattern of increasing displacement from the edge of the ellipse, called the *tip line loop* to the maximum displacement near the centre of the ellipse. As the faults propagate from a point source, they propagate more rapidly along the direction defined by the long axis of the ellipse. Fault tips at the ends of the long axis of the fault ellipse, horizontal for strike-slip faults, are *Mode II tips* where the direction of fault slip and fracture propagation are parallel. Fault tips at the ends of the short axis of the fault ellipse are *Mode III tips* where the direction of fault slip is perpendicular to the direction of fracture propagation. These tips are less common in horizontal map view for strike-slip faults. Secondary *Horsetail fractures* are curved fault splays near the end of Mode II tips that merge with the fault. They occur in the *extensional (dilational) quadrants* of faults ie. that side of the fault wall which is moving away from the tip and are associated with loss of displacement around the tips. In extensional quadrants, fractures often display a significant component of *Mode I* (opening) slip perpendicular to the fault plane combined with mode II slip parallel to the plane. They are called *mixed mode* fractures.

Extension fractures (T) are pure Mode 1 fractures. Chinnery (1966b - figure 4) identified secondary fault modes with more complex geometries, which were derived from an analogue modelling study (Chinnery, 1966a). *Type A* fractures represents the tendency for a strike-slip fault to extend (cf. 'splay faults' of Anderson, 1951), and include branching splay or horsetail fractures. *Type B* fractures are antithetic and conjugate to Type A, and commonly occur. Semi-circular *Type C* fractures intersect faults close to the tip but at a high angle and curve away towards the tip direction to become near parallel with the fault. Sometimes a third (higher) order of smaller fractures develops in response to movement on secondary fractures.

Wall zones are the volumes of rock adjacent to faults which undergo internal strains to accommodate the changes of displacement which occur along the fault. *Damage zones* are volumes of deformed wall rocks where the internal strains have caused the development of secondary faults, fractures and/or cleavages. Many secondary shear fractures are related to deformation of the rocks in the fault wall undergoing sympathetic shear deformation in the strike-slip regime. They are classified as *Riedel (R)*, *anti-Riedel (R´)* and *P* shears (Tchalenko, 1970) according to their orientation and sympathetic (R, P) or antithetic (R´) shear sense. In a right lateral system, R and P shears intersect the main fault surface at a low (20-30°) angle clockwise and anticlockwise of the fault respectively. R´ shears intersect the fault at a high angle (60-70°) clockwise from the fault. Other secondary fractures associated with movement on the fault are classified according to the scheme of Logan *et al.* (1979). *X* and *X´* fractures are conjugate shear fractures making angles of 60 - 70° to the fault and formed during shortening normal to the fault (Logan *et al.*, 1979). *Pinnate* fractures are en-echelon arrays that branch diagonally at angles of 40 - 60° from one side of a master fault. They commonly show dilation to form veins indicating an origin as Mode I fractures.

For normal faults, a *relay ramp* is an area of reoriented bedding which transfers displacement between two faults which overstep in map view and which have the same dip direction (Larsen, 1988). The definition was extended to strike-slip faults

affecting horizontal beds by Peacock and Sanderson (1995). Relay ramps may be breached by *bridging fractures* either synthetic or antithetic to the main faults.

In the examples discussed below, strike-slip faults affect steeply dipping beds. Map views of strike-slip faults frequently show the development of fault-bound *lens-shaped structures*. These structures may be compared with *sidewall ripouts* (Swanson, 1989), *open eye-structures* (Fossen and Hesthammer, 1997) or *strike-slip duplexes* (Woodcock and Fischer, 1986; Swanson, 1988; Cruikshank *et al.*, 1991). In cross-sections of normal fault systems where the axis of the relay is similarly perpendicular to the slip direction, similar structures are reported as *extensional duplexes*, *isolated lenses* or *closed loops* (Wernicke, 1981; Gibbs, 1984; Fossen and Gabrielsen, 1996;

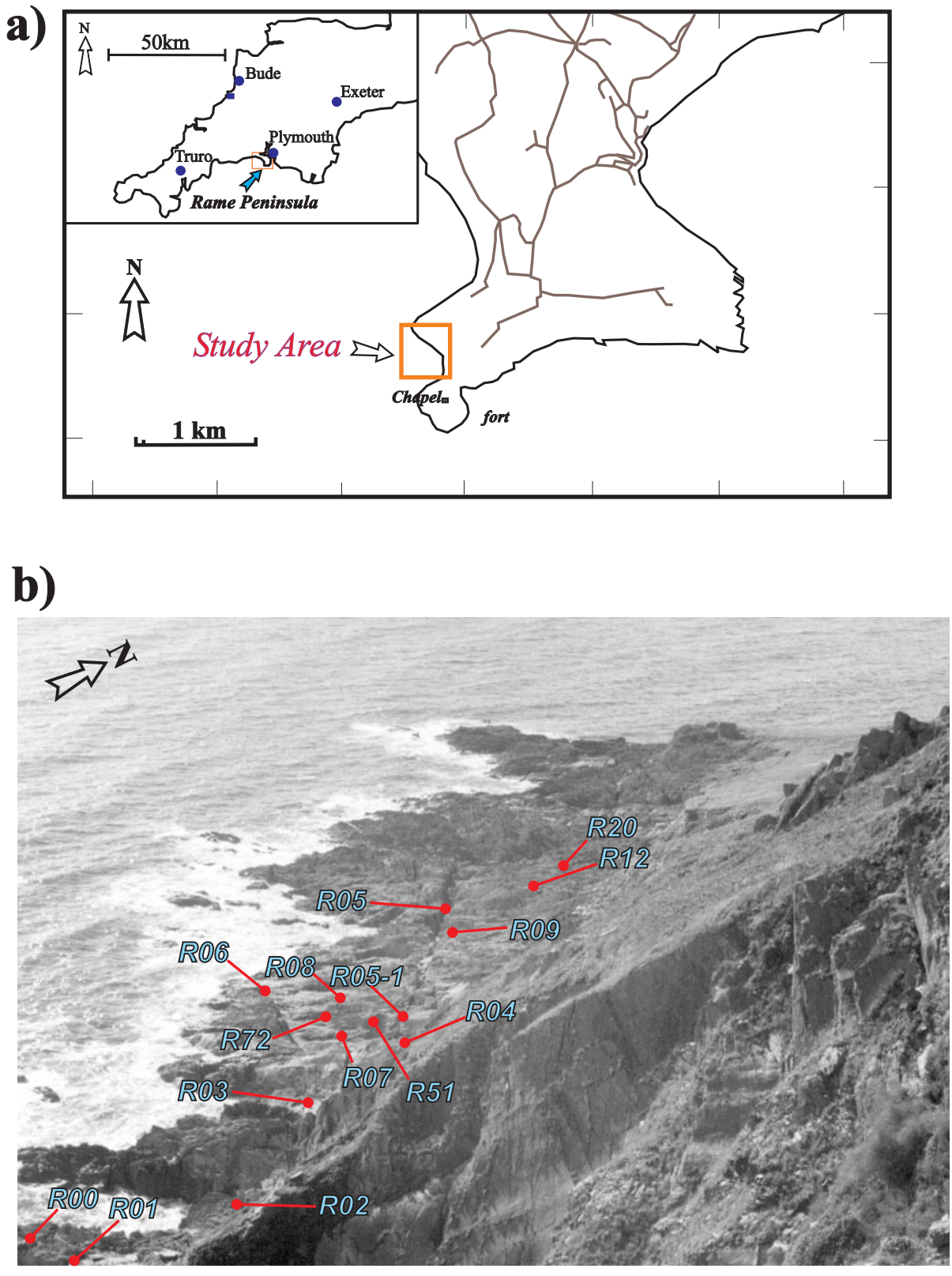

Figure 1. *Locality of the study area. a) Map showing the location of Rame Head (SX 417 487), southern Cornwall. b) Photograph showing the location of studied strike-slip faults within the boxed area in Figure 1a.*

Walsh *et al*., 1999). Fault linkage may be *hard-linked* (Walsh and Watterson, 1991) where the fault surfaces are linked on the scale of the map or cross section in use. *Soft-linked* faults are those between which there is a mechanical and geometric continuity achieved by ductile strain of the rock volume between them. They will appear to be isolated from one another on the scale of the map or section in use.

Rame Head

In any field study of strike-slip faults it is helpful to find steeply dipping or vertical markers by which separation or displacements can be determined. Good sites are hard to find but at Rame Head (Figure 1a) steeply dipping (70-90 º) beds at moderate to high angles to faults, provide good markers for determination of slip sense and displacement. The field site is a gently undulating wave-cut platform dissected by narrow erosional gullies (Figure 1b). Strike-slip faults show displacements of 0.1 ~ 5 m, and fairly straight overall traces. Most faults comprise several linked segments. They provide an opportunity to extend studies of low-displacement segmented faults at Crackington Haven (Kim *et al.,* 2000). The strike-slip faults show more complicated geometries than those at Crackington Haven as they are more evolved, i.e. they exhibit significantly higher maximum displacements relative to the length of the faults.

Detailed observation of the Rame Head faults, some characteristic damage structures and measured displacement (*d*) - distance (*x*) data provide a basis for the interpretation of *d-x* profiles. Numerous secondary faults and fractures in damage zones adjacent to the faults at Rame Head are classified and compared with those described from other study areas (Kim, 2000). Three damage propagation models for lens-shaped structures are suggested.

Research methods

Approximately 1:100 scale maps were made for whole fault systems and several maps at approximately 1:3 scale were made of tip damage zone. The maps were made from a mosaic of field photographs, which were adjusted using field measurements to reduce distortion.

In the field, direct measurement was made of the separation between marker beds across faults and the distance (*x*) along the fault from one tip to the marker beds. The separation is assumed to closely approximate the displacement (d) as shown by sub-horizontal slickenside striae, steeply plunging lines of intersection between conjugate faults and fractures and steeply plunging conjugate angular minor folds. The maximum displacement, usually near the centre of a fault, was also recorded if possible. In most cases faults are only partly exposed, so that the length from the tip of a fault to the maximum displacement was taken as a measure of the half-length of the fault length. The accuracy of measurement is ~10 mm for fault displacement, and ~100 mm for fault length because of surface relief. A further error may arise when integrating field data and photographic interpretations, due to the irregular nature of the exposure surfaces. Reference has been made to field measurements to minimise these errors.

Locality and geological setting

The studied area (SX 417 487; Figure 1) is a 300 m long stretch of the western coast of the Rame Peninsula between Queener Point and Rame Head Chapel. The host rock is interbedded slate and thin sandstone of the Boveysand Formation which lies within the Lower Devonian Meadfoot Group (Leveridge *et al*., in press). The slaty cleavage dips moderately to steeply southward throughout the area and is associated with early E-W major folds, inferred to be north- or upward-facing and gently east-plunging (Burton and Tanner, 1986). Several NW-SE trending strike-slip faults are related to the Portwrinkle and Cambeak-Cawsand fault zones (Burton and Tanner, 1986), and cut the penetrative cleavage and folding. Burton and Tanner (1986) suggest that the Portwrinkle fault acted as a transfer fault during early Variscan deformation.

The principal structures measured are bedding, right-lateral faults, subsidiary left-lateral conjugate faults, extensional veins, minor folds and slickenside striae (Figure 2). Bedding strikes ~ N075° and dips consistently steeply SE. Strike orientations of steep right-lateral faults are concentrated around N120°. Minor angular fold axes close to right-lateral faults plunge steeply SE, suggesting they were generated in response to fault displacements. Steep left-lateral faults concentrate around N035°.

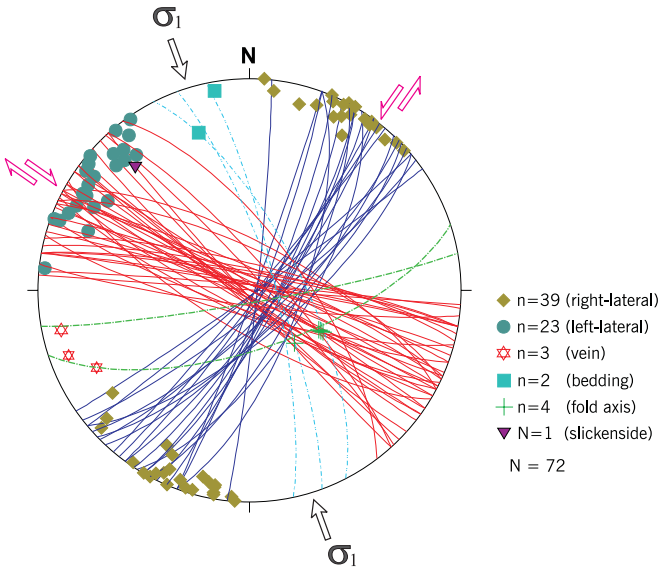

Figure 2. *Stereographic projection of bedding, strike-slip faults, veins, minor fold axes, and slickenside striae measured at Rame Head. The orientation of veins and palaeo* σ_1 *is about N160º.*

Field relationships show right-lateral faults are cut by left-lateral faults, but not *vice versa*. Some left-lateral faults terminate against right-lateral faults and *vice versa*. Evidence for the contemporary formation of both fault sets is equivocal but the combination of a steeply plunging line of intersection of damage zone faults and fractures (parallel to σ_2) and measurement of isolated extensional veins support a palaeostress σ_1 ~ N160° (Figure 2), consistent with a conjugate origin of the two sets of strike-slip faults. The absolute age of the faults is not constrained but it is likely that they were formed either during the main Variscan deformation or much later during Tertiary reactivation of earlier Variscan structures.

Description of strike-slip faults and damage zones

Maps of several faults showing damage structures are presented below. The faults are located in Figure 1b.

Fault R12

Figure 3a shows a 28 m long right-lateral left stepping segmented fault with an exposed tip at the north-western end. This tip is curved towards the dilational quadrant, with horsetail fractures defining a tip damage zone. Some segments are intersected by fractures making a high angle with the fault. The maximum displacement is ~ 320 mm. The corresponding ratio of d_{max}/L is about 0.01, a relatively low value compared with other faults in the area. The *d - x* profile (Figure 3b) has several peaks symptomatic of overlapping segments. Local minima are charactistic of contractional segment oversteps (e.g. Peacock, 1991). The slip minima around overstep zones are very similar to the relay structures in the normal fault zones, e.g. normal fault systems in the Bishop Tuff, Volcanic Tableland, California (Ellis and Dunlap, 1988).

Four segments (A - D) display a mixture of soft- or hard-linkage.

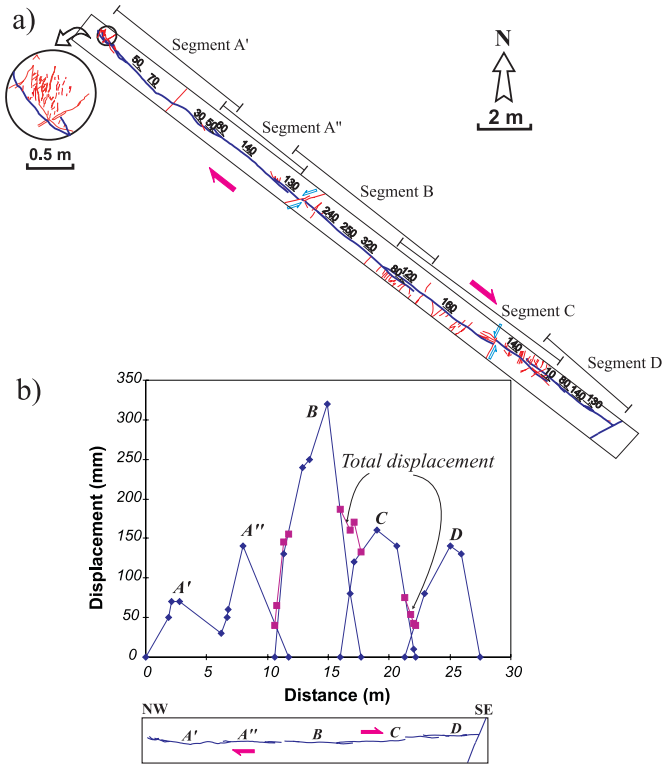

Figure 3. *a) Map showing a right-lateral fault (R12) with one tip and truncated against a fault. The maximum displacement is 320 mm in the middle part of the fault. Several overstep zones occur along the fault; some of them are hard-linked. The NW fault tip shows a horsetail splay fracture pattern (inset). Thick lines represent master faults and thin lines represent secondary faults and fractures for all the following maps. b) Map view and displacement (d) - distance (x) profile of fault R12; the minima characterise low displacements at relay zones. The small numbers and arrows denote displacement in mm along the fault for all the following maps.*

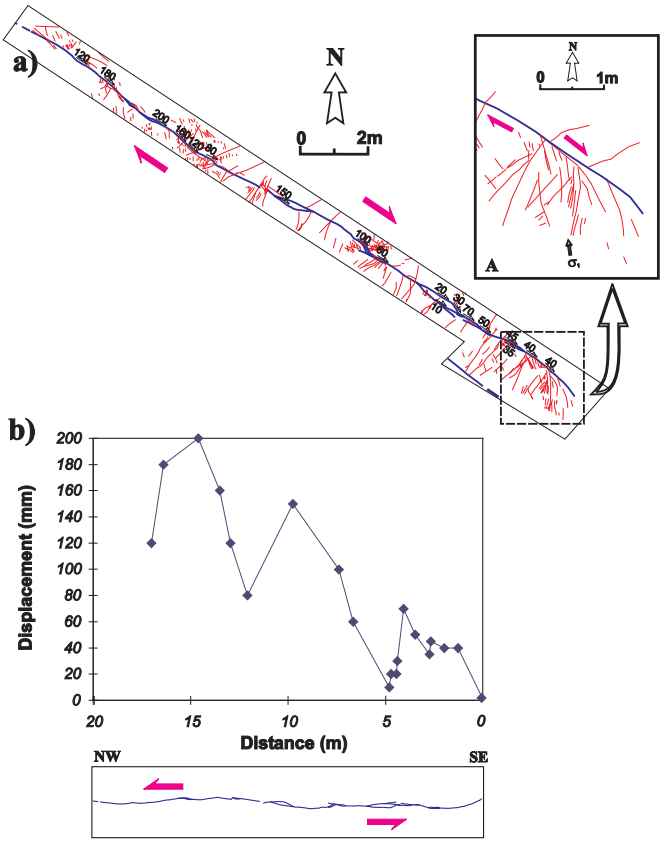

Figure 4. *a) Fault R09 consists of several linked segments separated by lens-shaped enclosures of wall rock. Displacement varies along the fault rising to a maximum value of 200 mm. Secondary fractures occur along the fault. In inset A, horsetail splay fractures are made up of extensional fractures and fractures intersecting the fault at high angles. b) Map view and displacement (d) - distance (x) profile of fault R09, showing several local minima and maxima along the fault, occurring at lens-shaped zones. The general trend of the profile shows that the displacement increases towards the NW then decreases.*

Segment *A* is divided into two hard-linked sub-segments (*A´* and *A´´*). They can be considered as two former isolated segments because the overall displacement at the linking point shows a minimum. Linkage has been facilitated by development of strike-slip relay ramps (Peacock and Sanderson, 1995). Displacement of most of the fault segments decreases generally from the centre towards the segment tips. Although not all the segments in this fault are hard-linked, the profile has a maximum displacement in the centre indicating the segments formed a coherent fault system. The mixture of soft-linked and hard-linked segments is characteristic of a fault system at an early stage of development.

Fault R09

This is one of the longest faults mapped ~30 m (Figure 4) and illustrates aspects of the more evolved nature of the faults at Rame Head. The ratio of d_{max}/L is about 0.007 for a maximum displacement of 200 mm. The master fault branches around several isolated lenses developed at bends or slight misalignments of fault segments, suggesting they were former relay ramps. Soft-linked segments occur in the middle of the fault and unlinked branch faults are developed around some lenses, which imply they were originally, isolated early fault tips. Only one tip of the master fault is exposed.

The exposed fault tip curves away southwards, with many horsetail fractures in the dilational quadrant. Inset *A* in Figure 4 shows typical extensional fracture (Mode I) dominant tip damage (Moore and Lockner, 1995; Vermilye and Scholz, 1999). The general trend of these extension fractures is consistent with a regional remote maximum compressive stress (σ_1) of N160° (Figure 2). Secondary fractures with a more clockwise trend may represent antithetic shears (R') at around N030° and high angle (X) shear fractures (Logan *et al.*, 1979) at around N060°. This tip damage pattern is typical of the horsetail splay style (e.g. Granier, 1985).

Displacement does not show a systematic distribution along the fault. The *d-x* profile shows several minima and maxima and is very low at branch faults and isolated lens zones indicating displacement transfer across to each splay fault. The two well-defined minima correspond to the position of two prominent lens-shaped structures.

Fault R02

This ~12 m long fault (Figure 5a) displays damage dominated by extension fractures at fault tips, and shear fractures (X) making a high angle to the main fault along the wall zone. Branch faults at both tips are curved towards the dilational quadrants (cf. Moore and Lockner, 1995; Vermilye and Scholz, 1999). Both tips have a zone of closely spaced secondary fractures in these dilational quadrants. At least two lens-shaped structures are developed along the fault.

Displacement generally decreases towards both fault tips from the centre, with rapid decreases in displacement occurring just before the branch faults at both tips. The maximum displacement (520 mm) occurs just before the prominent branch faults at the SE tip. Here the northern branch fault appears to transfer displacement through linkage to an adjacent unexposed fault that would continue eastwards as the displacement starts to increase again eastward (from 40 mm to 50 mm). At the north-

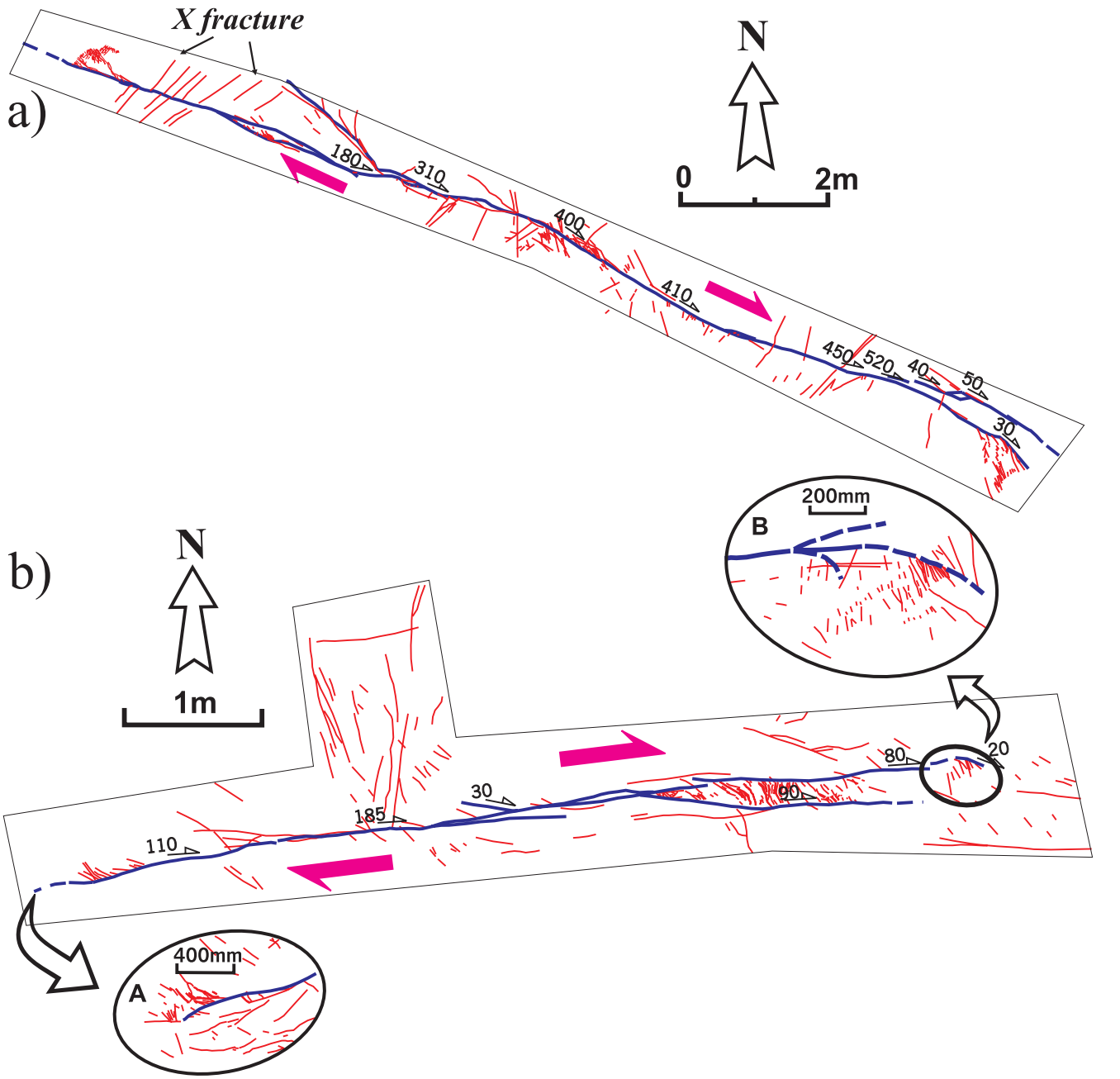

Figure 5. *a) Map of Fault R02. Horsetail splay tip damage fractures occur at both fault tips, and branch faults and high angle fractures are present along the central section. The fault rapidly loses displacement where it branches. b) Fault R01 shows horsetail splay tip damage fractures at both tips (insets). The fault develops a prominent splay at its eastern termination. The wedge-shaped block between these two faults is rotated and veined. The vein arrays show dextral sigmoidal shapes.*

western end, displacement rapidly decreases from ~310 mm to ~180 mm where the fault branches. Two branch faults form a wedge-shape structure but without extensive fracturing and/or rotation despite the large displacement gradient.

Fault R01

This ~ 7 m long fault (Figure 5b) is characterised by damage consisting of extension fractures at fault tips and branch fractures in the central section. Extension fractures occur at the tips in the dilational quadrants, parallel to the remote σ_1 (~ N160°). The eastern tip terminates with a prominent branch fault to form a fork-shaped structure. Within the enclosed wedge-shaped block, several minor secondary cross fractures are developed, and are now rotated to show sigmoidal shapes filled with vein quartz. The displacement generally decreases from ~ 185 mm at the centre towards both fault tips, giving a ratio of d_{max}/L about 0.028, significantly higher than faults R12 and R09.

Fault R07

Two sub-parallel left-lateral faults (Figure 6a) interact as indicated by the *d-x* profile which shows conservation of displacement where they overlap (Figure 6b). The maximum displacements for the two faults are ~ 350 mm and ~ 130 mm, giving a ratio of d_{max}/L of about 0.035 and 0.033, respectively.

The 10 m long fault displays a set of lens-shaped structures and some unlinked branch faults. Lens-shaped structures coincide with steps in the fault trace. Detail in the *d-x* profile brings out the effect of the largest lens-shaped structure. For *Fault A* a pronounced minimum occurs and the sum of the displacement of the two branches shows a somewhat depressed pattern hereabouts. The minor sub-parallel *Fault B* mirrors the overall pattern. The effect is to produce a strike-slip duplex (Woodcock and Fischer, 1986; Swanson, 1988; Cruikshank *et al.*, 1991). There are few

secondary fractures and no evidence of localised leading edge or trailing edge damage as might be expected if the lenses developed as rip-outs (Swanson, 1988). The *d-x* pattern is typical of interaction between normal fault segments transferring displacement (Huggins *et al*., 1995).

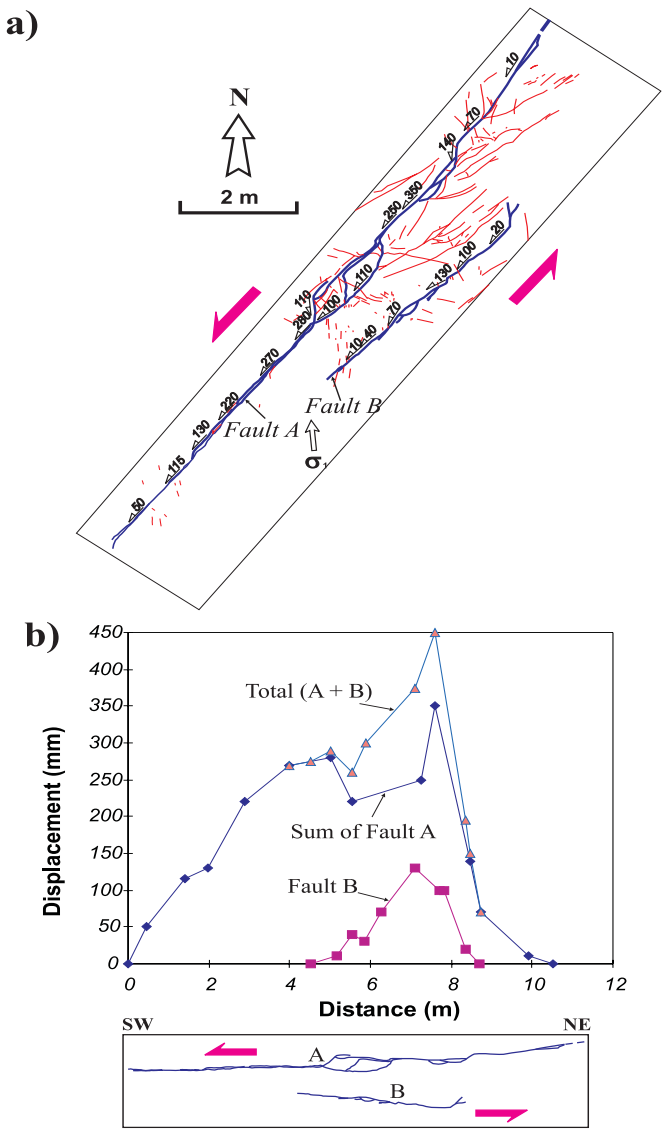

Figure 6. *a) Two sub-parallel left-lateral faults (R07). Eight lens-shaped structures occur along this fault system. The major fault shows a dominance of dilational left-stepping segment linkage leading to the development of strike-slip duplexes. b) Displacement (d) - distance (x) profile of fault R07. The major fault (A) shows a displacement minimum in the middle of the profile near a lens-shaped structure. The total displacement also shows a minimum.*

Fault R03

This 10 m long right-lateral fault (Figure 7) shows a complex geometry, dominated by two fault bounded lenses. The fault maintains an approximately constant displacement, so the tips probably lie some distance from either end of the exposure. The two lenses are located on either side of the main strand of the fault with the largest displacement. The western lens (left stepping) is predominantly contractional and the eastern lens (right stepping) dilational. The intensity of fracturing around the eastern lens is lower, reflecting its positioning in a dilational environment.

The shape of the lenses has resulted in localised stress concentrations of opposite sign, giving rise to structures classified as releasing or restraining (Christie-Blick and Biddle, 1985; Sibson, 1989). The nearfield stress distribution and a simple kinematic model is shown in inset *B* (Figure 7). Localised damage patterns reflect these settings. Secondary extension (T) and high angle (X) fracture patterns are predominant (inset *A* in Figure 7). Many extension fractures and veins are developed around western lens, with a very high fracture density around the north-western perimeter. Semi-circular fracture patterns occur in the northern wall of the western lens-shaped structure. This type of fracture pattern has been reproduced as *Type C* by Chinnery (1966b) in a numerical modelling study.

Damage patterns

The damage around faults can be classified into that occurring on either side of the main fault strand (wall zone damage), around the fault terminations (tip zone damage) and where relay structures link en-echelon fault segments together (linking zone damage).

Wall zone damage

High angle shear fractures and higher order secondary fractures predominate (e.g. Figure 4). Fractures intersecting the fault at a moderate angle occur around both restraining and releasing fault bends and lens-shaped structures, showing evidence of local extension. The two faults in Figure 8 display wall zone damage structures and are good examples of patterns observed around most of the faults described in the study area. *R04* (Figure 8a) is confined between two later left-lateral faults whilst *R51* (Figure 8b) is a small subsidiary fault parallel to *R05-1* (Figure 10a). Several lens-shaped structures and some branch faults are developed along the faults.

In fault *R04* (Figure 8a) there are many secondary antithetic fractures at a high angle to the master fault (X fractures). The slip sense of X fractures is left-lateral as indicated (Figure 8a, insets *B* and *C)* by the offset of beds and the development of tip cracks. Minor high angle fractures (X) or higher order fractures (Figure 8a, inset A) link to form pull-aparts in relay zones. Secondary fractures are slightly reoriented inferring the local opening directions and therefore local σ_3 are not parallel to those of secondary fracture orientations associated with the master fault system.

Antithetic fractures (X) dominate along the wall zone around fault R51 (Figure 8b) whilst lower angle antithetic fractures (R) or extensional fractures (T) become dominant towards the fault tip.

Tip zone damage

Tip damage is dominated by horsetail fractures (Figures 4 - 6), splay faults and antithetic shear fractures (R¢). Good examples of tip zone damage are shown in Figure 9. For example, the fault in Figure 9a terminates with two short splay faults on the west side, which pass into arrays of antithetic shear fractures. Semi-circular fractures occur near the termination of the main fault. They resemble *Type C* fractures of Chinnery (1966b). Damage around the fault tip in Figure 9b can also be resolved into branch and antithetic shear fractures (*Type A* and *B* fractures of Chinnery, 1966b). At the end of the tip zone, small NW trending linear fractures occur without any indication of shear displacement. These are extension fractures parallel to the far-field orientation of σ_1 (Figure 2).

Branch faults may isolate wedge-shaped blocks within which arrays of fractures strike at near perpendicular angle to the main structure. In Figure 9c, within the wedge-shaped block bounded by the two splays, there are two predominant secondary fracture trends. One set consists of pinnate (T) extension fractures along both side-walls of the splay faults. The other set of fractures have been deformed to sigmoidal shapes by continued movement along the splay faults. Although an antithetic sense of these fractures is not obvious, left-lateral shear can be inferred from higher order tip cracks. Barren (extension?) fractures terminate against the antithetic fractures implying later formation.

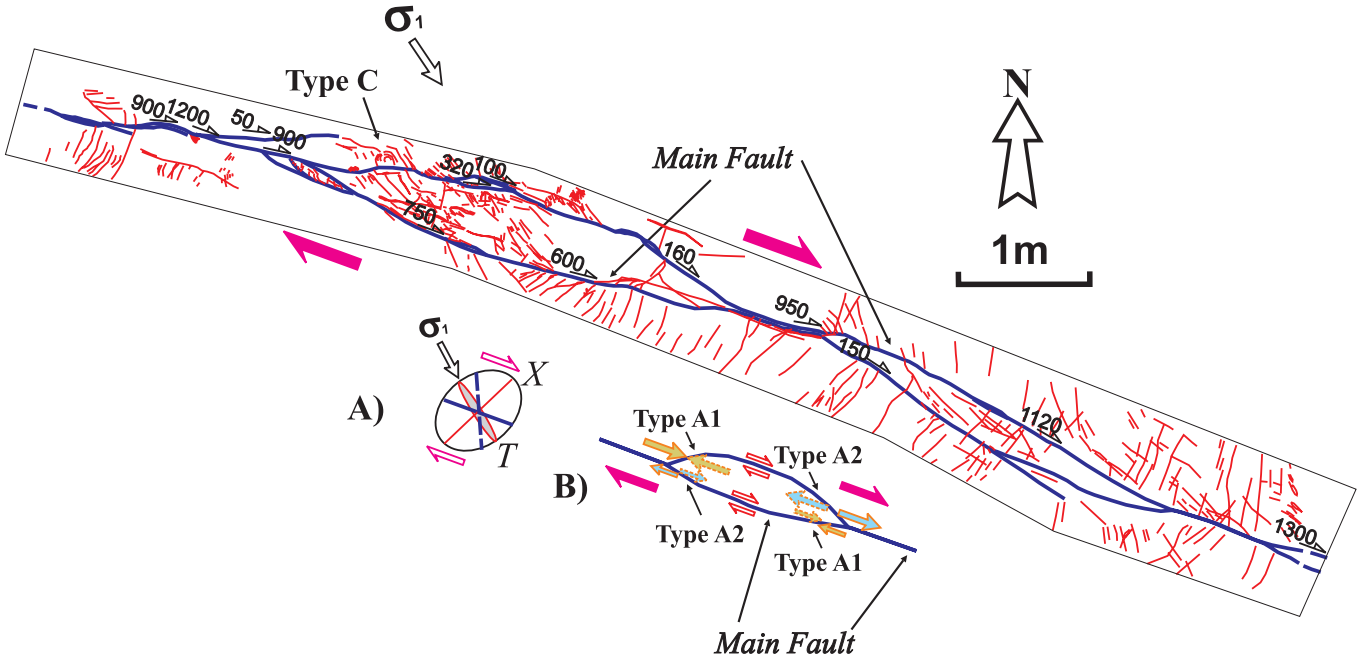

Figure 7. *Map view of a right-lateral fault (R03) displaying two prominent lens-shaped structures. Several branch faults intersect the main fault at former segment tips. Many secondary fractures are present along the fault with orientations corresponding to type A and C of Chinnery (1966b), extensional fractures (mode I) and high angle (X) fractures. Inset A shows a stress ellipse indicating maximum compressive stress and other fracture patterns. Inset B shows local stress distribution around bends and lens-shaped structures (Swanson, 1989).*

Linking zone damage

This section documents the effects of variation in the geometry of relay ramps upon damage structures. Figure 10 shows three examples of different patterns of linkage geometry. In the example shown in Figure 10a antithetic faults are almost perpendicular to two obliquely interacting fault tips. Figure 10b and 10c show hard-linkage of two misaligned segments. In Figure 10b the eastern segment developed horsetail splays which are linked with the western segment. This relay zone produces a fault bend rather than a lens-shaped structure. Figure 10c shows a hard-linked relay zone developed due to a misalignment between two right-lateral faults. After linkage, further slip promoted opening on the fault bends (cf. dilational jog, Sibson, 1989) creating open spaces filled with vein quartz. Secondary extension fractures (or R¢ shear fractures) occur around and within the lens-shaped structure. Lens-shaped structures commonly occur along faults (Figures 4 - 8 and 10c). The shape ratio (short axis/long axis) of the structures ranges between 1:3 and 1:10. Associated fracture patterns include branch faults and semi-circular fractures. Veins occur at fault bends and leading/trailing edges.

Discussion

Wall zone damage

High angle (X) fractures (Logan *et al.*, 1979) are common along fault walls (Figures 5a, 7a and 8). Bartlett *et al.* (1981) suggested, from analogue modelling, that high angle (X) shear fractures are not common in early stages of fault evolution but initiate in the post-peak stages, when fracture zones contain a higher percentage of R shears, P shears and gouge. It follows that high angle (X) fractures develop in wall zone of mature faults and R¢ or T fractures are predominant around fault tips and relay zones.

Passive rotation of early formed fractures can also generate high angle fractures. In a fault zone of finite width defined by a zone of distributed shear strain, secondary faults or fractures will tend to rotate as passive markers during further shear strain (Arboleya and Engelder, 1995). The amount of rotation depends on the amount of displacement and on the initial orientation of each subsidiary fracture (Ramsay and Huber, 1987; Arboleya and Engelder, 1995). Rotation of R¢ shears may lead to fractures with the same orientation as later generated X fractures.

Pinnate-style fractures and veins may develop as wall zone damage (Figure 9c). These are en-echelon structures that branch diagonally from one side of a master fault. Some pinnate fractures are veins or synthetic Riedel shears but others are conjugate, antithetic shears at about 60° ~ 90° to the master fracture (Hancock, 1972).

Tip damage

Tip damage structures at Rame Head are noteworthy because the strike-slip faults in this study area show significant displacements and more complicated fracture patterns than less evolved strike-slip systems e.g. at Crackington Haven (Kim *et al.*, 2000). Tip damage is considerably enhanced at segment linking zones. Many features can be readily understood and interpreted from theoretical considerations and from both analogue and numerical experiments.

As a master fault propagates, secondary fractures are generated releaving stress concentrations caused by high displacement gradients, especially at fault tips (McKinstry, 1953; Chinnery, 1966a, 1966b). At the tips, the master faults curve towards the dilational quadrants (Figures 3a, 4a and 5) (Moore and Lockner, 1995; Vermilye and Scholz, 1999) and commonly terminate as horsetail splay fractures and veins (Figures 3a, 4a and 5).

Near Mode II fault tips, the predominant sliding mode causes fracturing to initiate obliquely to the fault plane forming horsetail splay fractures (McKinstry, 1953; Chinnery, 1966b; Freund, 1974; Arthaud and Matte, 1977; Petit and Barquins, 1988). Linear elastic fracture mechanics theory predicts a concentration of stresses near Mode II tips that promotes the initiation of secondary single (e.g. Broek, 1991; Lawn, 1993) or multiple splay fractures (e.g. Cooke, 1997), which are opening-mode fractures obliquely oriented to the principal fault. Theoretical prediction of the propagation paths of these fractures has been verified by laboratory experiments (Brace and Bombolakis, 1963; Erdogan and Sih, 1963; Nemat-Nasser and Horii, 1982; Thomas and Pollard, 1993), which show that extension fractures propagate in the direction parallel to the near-field σ_1 (Segall and Pollard, 1983).

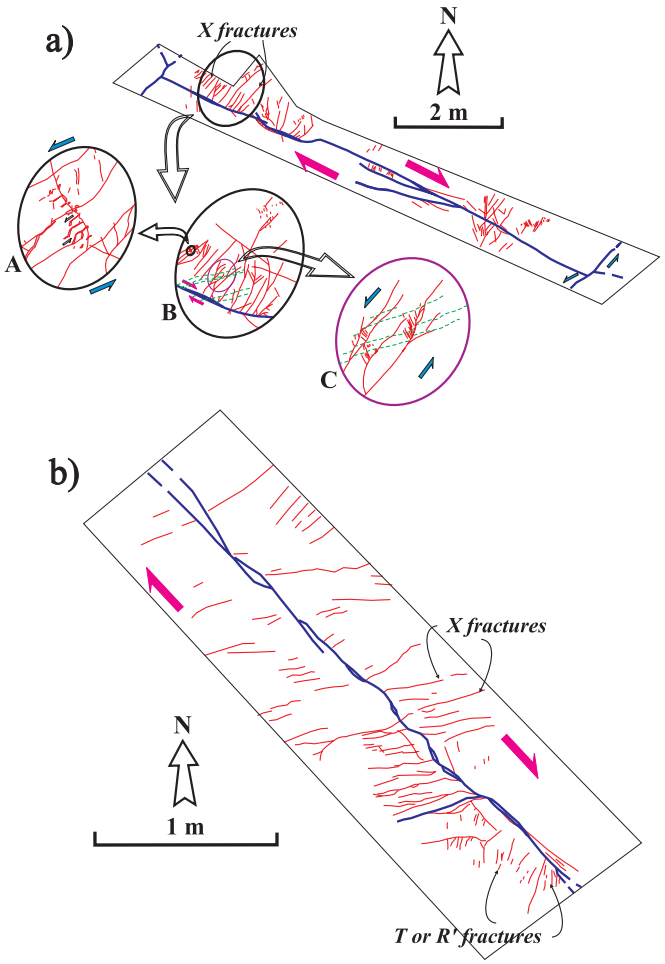

Figure 8. *Wall zone damage structures. a) Map of a right-lateral fault (R04); the master fault is at least 14 m long. It is truncated at the northwestern end and displaced by a later NE-SW trending fault towards its eastern end. Branch faults are developed along the middle of the section. Dotted lines denote bedding. Insets show details of fracture arrays. b) Map view of a 3 m section of a fault (R51) displaying wall zone damage structures. The fault tip lies about 2 m to the south-east of the map. The fracture pattern changes from high angle fractures (X) to lower angle antithetic fractures (RN) or extensional fractures (T) at the fault tip.*

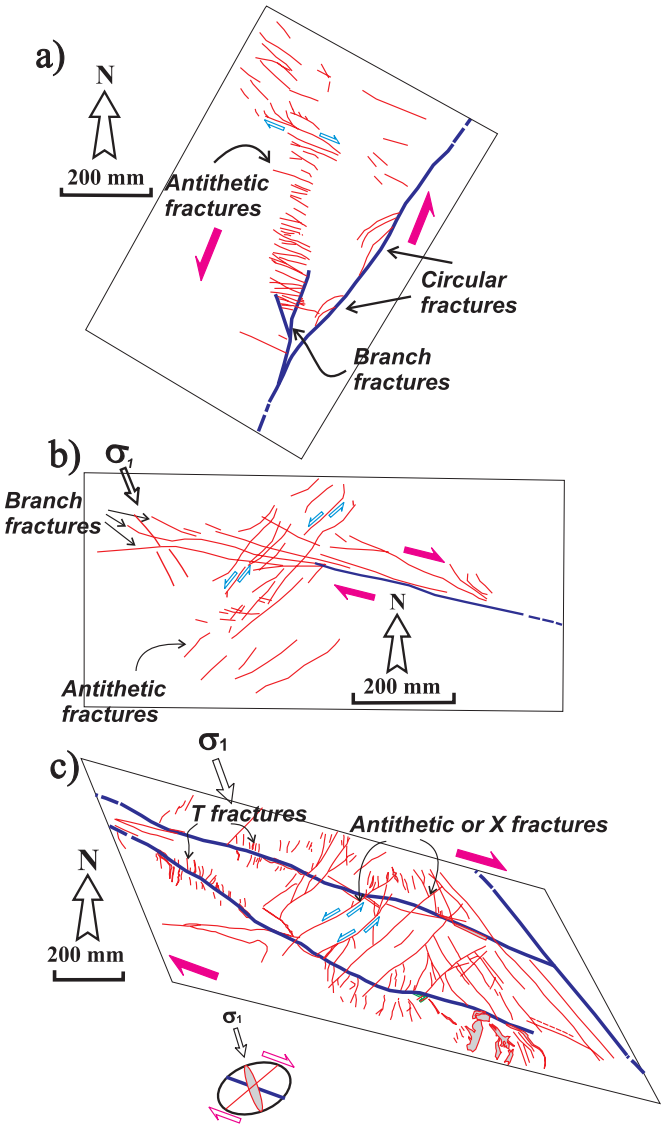

Figure 9. *Tip zone damage structures. a) Map view of tip damage structures at the termination of left-lateral fault R20 . Antithetic shear fracture arrays are developed between branch faults. b) Tip damage at the termination of fault R08 consisting of several splay faults, extensional fractures and antithetic fractures. c) Wedge-shaped block between two ~ 1 m long right-lateral faults that form splays at the termination of a larger fault. Antithetic faults are developed within the wedge-shaped block, subsequently deformed to sigmoidal shapes by continuing right-lateral shear. Arrays of extensional pinnate fractures occur along both side-walls of the splay faults.*

Figures 4a, 5 and 9 show Type A branching splay fractures (Chinnery, 1966b). Type B antithetic fractures occur commonly (Figure 9). The semi-circular Type C fractures occur around some fault tips including old segment tips (Figure 7 and 9a). Type B fractures can be divided into two groups, R¢ shears and high angle (X). They arise from the conjugate directions of shearing associated with local near-field stress reorientation. R¢ shears are dominant at tip zones (Kim *et al.*, in press).

Overstep zones and lens-shaped structures

High-angle fractures form long antithetic linking faults in overstep zones(Figure 10a). These can be either slightly rotated R¢ fractures or high angle (X) fractures. These bridging fractures can facilitate subsequent block rotation as in Figure 9c where the wedge-shaped area between the two faults is rotated by further movement along the main faults, causing movement on antithetic shear fractures (R¢ or type B of Chinnery, 1966b). Similar fracture patterns have been described from Gozo, Maltese Islands (Kim *et al.*, in press). In most Rame Head examples, antithetic cross-fractures are generated as R¢ shears.

Lens-shaped structures in strike-slip fault system may be analogous with strike-slip duplexes (Woodcock and Fischer, 1986; Swanson, 1988; Cruikshank *et al.*, 1991), sidewall ripouts (Swanson, 1989) and open eye-structures (Fossen and Hesthammer, 1997). Three possible mechanisms and evolution are suggested for the development of lens-shaped structures (Figure 11). In model one (Figure 11a) two fault segments approach towards each other (stage 1). At the relay ramp between adjacent fault segments, the segments branch and the branches propagate to eventually breach the relay (stages 2 and 3) (Figure 3a). After one segment tip links to the other segment, the other segment tip propagates further (Figures 3a, 4a and 8b). This free tip is curved and eventually links with the other segment, producing a lens (stage 4) (Figure 10c). By subsequent displacement along the fault, further fractures are generated within and/or outside the lens to form a strike-slip duplex (stages 5-7) (Figure 6a). The connecting faults can form different patterns and shapes of differing degrees of complexity (Cruikshank *et al.*, 1991). Displacement along the fault is partitioned between bridging fractures at lens-shaped structures.

In the second model for lens-shaped structures (Figure 11b) a section of a fault sticks causing a secondary fracture to develop

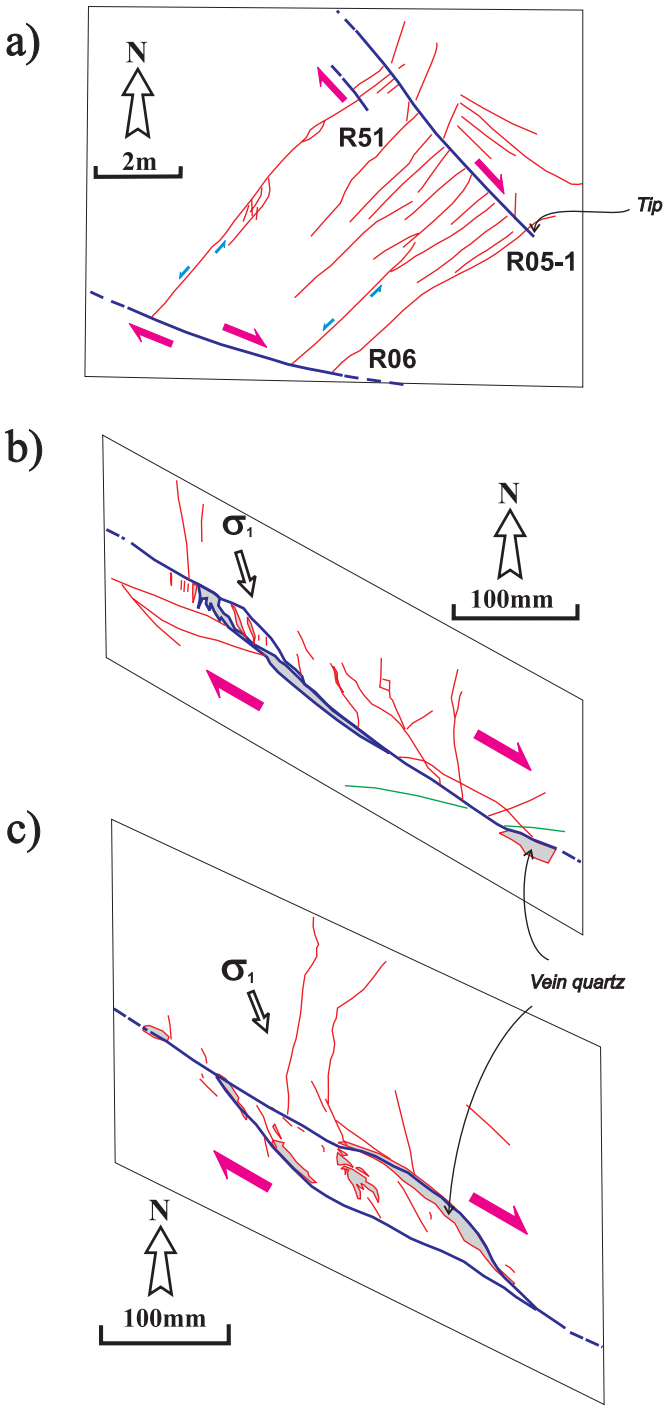

Figure 10. *Linking zone damage structures. a) A dilational overstep between two right-lateral faults R05-1 and R06. Fault R05-1 terminates to the SE and transfers displacement onto Fault R06. A series of linking antithetic faults almost perpendicular to the main faults are developed in the overstep zone. The antithetic faults have left-lateral displacements up to 350 mm. b) Map of a dilational linkage zone between two non-parallel fault segments. The site of one of the former segment fault tips shows a horsetail fracture pattern and the other shows veins filled with quartz. The two segment tips are hard-linked and extensive open spaces are filled with quartz at the fault bends. Fault R072-1 is next to fault R072. c) Lens-shaped dilational overstep structure at a dilational linkage zone (R072). Secondary fractures occur around and within the structure. Open spaces formed by dilation are filled with quartz.*

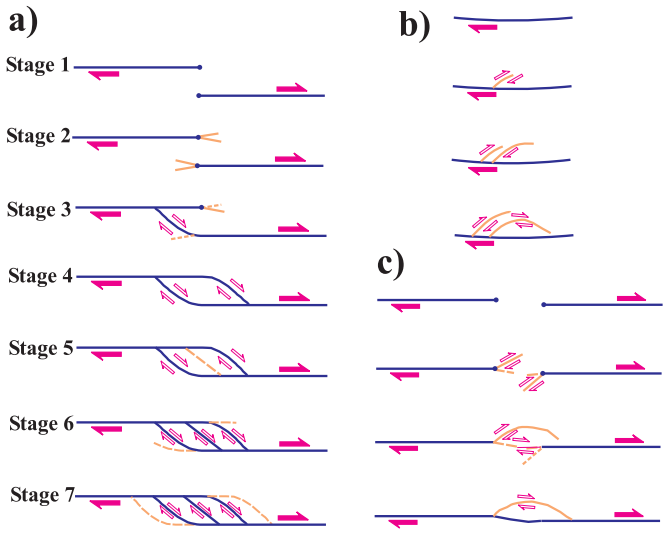

Figure 11. *Three alternative models for the development of lens-shaped structures. a) The isolated lens originates from an overstep and evolves into a strike-slip duplex (modified from Woodcock and Fischer, 1986). b) The isolated lens originates from semi-circular secondary fractures similar to a sidewall ripout (Swanson, 1989). c) The isolated lens originates from misaligned segments with secondary fractures, such as branch faults in overstep zones.*

and transfer the displacement onto itself. This leads to sidewall ripouts (Swanson, 1989). This mode of formation is characterised by relatively little damage within the lens-shaped structure and an asymmetric shape. Some Rame Head faults show semi-circular type C fault branches (Figures 7 and 9a), which could be precursors to ripout development.

A third type of lens-shaped structure may form where there is a slight misalignment of two fault segments (Figure 11c, 3a). Linking by a combination of propagation of fault tips and branch faults leads to the formation of asymmetric lenses (Figure 7).

Relationship between strike-slip fault geometry and displacement

The *d-x* profiles of strike-slip faults in the study area are highly variable as are those in other strike-slip fault systems (Peacock, 1991). The variability is too large to simply be attributed to measurement errors. Most of the profiles are highly asymmetric, showing higher displacement gradients and displacement minima at oversteps, lens-shaped zones or branching zones (Figures 3b, 4b and 6b). Asymmetry and displacement minima in displacement profiles are typically associated with segment linking and fault branching (e.g. Ellis and Dunlap, 1988). Interaction between segments prior to linkage results in accentuation of displacement gradients in the region of segment overlap (Walsh and Watterson, 1990; Peacock, 1991; Peacock and Sanderson, 1991; Trudgill and Cartwright, 1994; Huggins *et al.*, 1995; Fossen and Hesthammer, 1997). Displacement profiles showing irregular distributions along strike mark interactions between adjacent segments (Peacock, 1991) through horsetail faults and lens-shaped structures. At Rame Head the complex distribution can be modelled by a fault growth history involving the lateral propagation and linkage of early-formed segments.

Lens-shaped structures at Rame Head are characterised by displacement minima and are consistent with an origin by linkage of fault tips. As the faults evolve, early irregularities are smoothed out and the overall *d-x* profile becomes simpler, as has been described for normal faults (Dawers and Anders, 1995). Lens-shaped structures formed by ripouts are unlikely to generate displacement minima if they develop as envisaged by Swanson (1989).

The large range of lateral displacement gradients in faults is mainly due to interactions between neighbouring faults (Peacock, 1991). Additional complexities may result from local

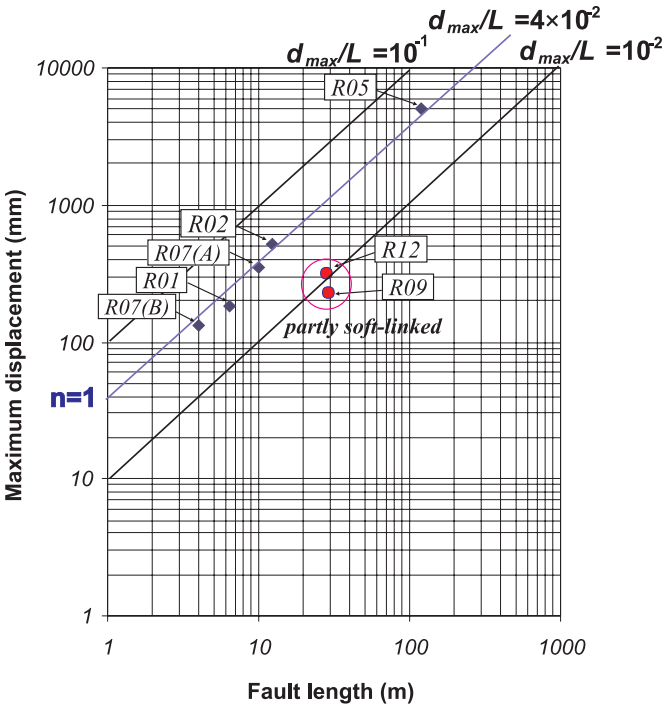

Figure 12. *Maximum displacement - fault length (d_{max}/L) relationship for all measured strike-slip faults in the study area. Diamonds are for hard-linked faults; circles for partly soft-linked faults. The ratio of d_{max}/L is lower for the partly soft-linked faults than for the hard-linked faults.*

variations in remote stresses and the frictional properties of the fault surfaces (Bürgmann *et al*., 1994), from the distribution of friction coefficient (Cooke, 1997) and from processes related to non-planar or discontinuous segment linkage (Peacock, 1991; Peacock and Sanderson, 1991; Bürgmann *et al*., 1994; Cartwright *et al*., 1995, 1996; Fossen and Hesthammer, 1997; Cartwright and Mansfield, 1998). Slip along a fault may also vary as a result of lithologic variations (Bürgmann *et al*., 1994).

Maximum displacement / fault length (d_{max}/L) relationship

The general expression of the relationship between the maximum cumulative displacement on a fault (d_{max}) and the fault trace length (L) is given as;

$$d_{max} = cL^n,$$

where the value of c is dependent on rock properties and the range of the exponent value, n, is from 1 to 2 (Kim *et al*., 2000). The relationship of d_{max}/L for measured strike-slip faults in the study area is plotted in Figure 12. The trace lengths plotted are for fault zones, where the overall displacement is conserved by summing the displacements on fault segments which are hard and soft-linked. Even though data are only available for seven faults, the distribution shows evidence for the pattern of fault growth. Most of the data have values of d_{max}/L lying between 10^{-1} and 10^{-2}; two partly soft-linked faults plot near $d_{max}/L = 10^{-2}$, with hard-linked faults plotting near $d_{max}/L = 4 \times 10^{-2}$. The hard-linked faults lie on a line of slope $n = 1$. From this result, two main points can be made: 1) The faults R01, R02, R05, R07(A) and R07(B) are hard-linked faults forming a geometrically coherent system; 2) If a fault system has evolved to a hard-linked fault zone, displacement is concentrated along master faults (Sibson, 1989; Cowie and Scholz, 1992). Partly soft-linked faults (R12 and R09; Figures 3a and 4a) have lower ratios of d_{max}/L. This suggests that faults grow through segment linkage (e.g. Peacock and Sanderson, 1991), and that displacement is concentrated on the master fault as it increases. This result is similar to that obtained from Crackington Haven (Kim *et al*., 2000). Therefore the argument for the 'step-like growth path' model (Cartwright *et al*., 1995; Kim *et al*., 2000) is applicable to these hard-linked strike-slip faults.

Conclusions

1. Several metres to tens of metres long right-lateral faults strike WNW-ESE. Antithetic NE-SW left-lateral faults are also developed. The remote maximum compressive stress (σ_1) forming these fault sets is about N160E. Veins (Mode I fractures) are parallel to this orientation.
2. Most of the faults show Mode II tip styles at which damage structures are dominated by horsetail splay fractures making a low angle (20-30°) to the main fault.
3. Damage in the walls is dominated by high angle fractures (60-70°) (X or RN).
4. Many fault segments are linked by lens-shaped structures. The shape ratio (short axis/long axis) of the structures ranges between 1:3 and 1:10.
5. If the fault system as a whole is considered, the *d-x* relationship resembles that for a hard-linked fault. Local displacement minima occur at relay ramps, lens-shaped structures or branch faults. Displacement rapidly decreases at lens-shaped structures, suggesting that they are developed from segment fault tips and relay zones.
6. The maximum displacement / fault length (d_{max}/L) plot for the strike-slip faults is higher for hard-linked faults with lens-shapes structures ($\sim 4\times10^{-2}$) than for soft-linked faults ($\sim 1\times10^{-2}$).

Acknowledgements

We thank David Peacock for his constructive comments on the manuscript.

References

ANDERSON, E.M. 1951. *The Dynamics of Faulting.* Olivier and Boyd, Edinburgh.

ARBOLEYA, M.-L. and ENGELDER, T. 1995. Concentrated slip zones with subsidiary shears: their development on three scales in the Cerro Brass fault zone, Appalachian Valley and Ridge. *Journal of Structural Geology,* **17**, 519-532.

ARTHAUD, F. and MATTE, Ph. 1977, Late Palaeozoic strike slip faulting in southern Europe and northern Africa: result of a right lateral shear zone between the Appalachians and the Urals. *Geological Society America Bulletin,* **88**, 1305-1320.

BARTLETT, W.L., FRIEDMAN, M. and LOGAN, J.M. 1981. Experimental folding and faulting of rocks under confining pressure. Part IX. Wrench faults in limestone layers. *Tectonophysics*, **79**, 255-277.

BRACE, W.F. and BOMBOLAKIS, E.G. 1963. A note on brittle crack growth in compression. *Journal of Geophysical Research,* **68**, 3709-3713.

BROEK, D. 1991. *Elementary Engineering Fracture Mechanics.* Kluwer Academic, Norwell, Boston.

BURGMANN, R., POLLARD, D.D. and MARTEL, S.J. 1994. Slip distributions on faults: effects of stress gradients, inelastic deformation, heterogeneous host-rock stiffness, and fault interaction. *Journal of Structural Geology,* **16**, 1675-1690.

BURTON, C.J. and TANNER, P.W.G. 1986. The stratigraphy and structure of the Devonian rocks around Liskeard, east Cornwall, with regional implications. *Journal of the Geological Society, London,* **143**, 95-105.

CARTWRIGHT, J.A. and MANSFIELD, C.S. 1998. Lateral displacement variation and lateral tip geometry of normal faults in the Canyonlands National Park, Utah. *Journal of Structural Geology*, **20**, 3-19.

CARTWRIGHT, J.A., MANSFIELD, C.S. and TRUDGILL, B.D. 1996. Fault growth by segment linkage. In: BUCHANAN, P.C. and NIEUWLAND, D.A. (eds), *Modern developments in structural interpretation, validation and modelling*. Special Publication, Geological Society, London, **99**, 163-177.

CARTWRIGHT, J.A., TRUDGILL, B.D. and MANSFIELD, C.S. 1995. Fault growth by segment linkage: an explanation for scatter in maximum displacement and trace length data from the Canyonlands Grabens of SE Utah. *Journal of Structural Geology,* **17**, 1319-1326.

CHINNERY, M.A. 1966a. Secondary faulting: I. Theoretical aspects. *Canadian Journal of Earth Sciences*, **3**, 163-174.

CHINNERY, M.A. 1966b. Secondary faulting: II. Geological aspects. *Canadian Journal of Earth Sciences,* **3**, 175-190.

CHRISTIE-BLICK, N. and BIDDLE, K.T. 1985. Deformation and basin formation along strike-slip faults. In: BIDDLE, K.T. and CHRISTIE-BLICK, N. (eds), *Strike-slip Deformation, Basin Formation, and Sedimentation*. Society of Economic Palaeontologists and Mineralogists, Special Publication, **37**, 1-34.

COOKE, M.L. 1997. Fracture localization along faults with spatially varying friction. *Journal of Geophysical Research,* **102**, 22,425-22,434.

COWIE, P.A. and SCHOLZ, C.H. 1992. Physical explanation for the displacement-length relationship for faults using a post-yield fracture mechanics model. *Journal of Structural Geology,* **14**, 1133-1148.

CRUIKSHANK, K.M., ZHAO, G. and JOHNSON, A.M. 1991. Duplex structures connecting fault segments in Entrada Sandstone. *Journal of Structural Geology*, **13**, 1185-1196.

DAWERS, N.H. and ANDERS, M.H. 1995. Displacement-length scaling and fault linkage. *Journal of Structural Geology,* **17**, 607-614.

ELLIS, M.A. and DUNLAP, W.J. 1988. Displacement variation along thrust faults: implications for the development of large faults. *Journal of Structural Geology*, **10**, 183-192.

ERDOGAN, F. and SIH, G.C. 1963. On the crack extension in plates under plane loading and transverse shear. *Journal of Basic Engineering,* **85**, 519-527.

FOSSEN, H. and GABRIELSEN, R.H. 1996. Experimental modelling of extensional fault systems by use of plaster. *Journal of Structural Geology*, **18**, 673-687.

FOSSEN, H. and HESTHAMMER, J. 1997. Geometric analysis and scaling relations of deformation bands in porous sandstone. *Journal of Structural Geology,* **19**, 1479-1493.

FREUND, R. 1974. Kinematics of transform and transcurrent faults. *Tectonophysics*, **21**, 93-134.

GIBBS, A.D. 1984. Structural evolution of extensional basin margins. *Journal of Geological Society, London,* **141**, 609-620.

GRANIER, T. 1985. Origin, damping and pattern of development of faults in granite. *Tectonics,* **4**, 721-737.

HANCOCK, P.L. 1972. The analysis of en-echelon veins. *Geological Magazine,* **109**, 269-276.

HUGGINS, P., WATTERSON, J., WALSH, J.J. and CHILDS, C. 1995. Relay zone geometry and displacement transfer between normal faults recorded in coal mine plans. *Journal of Structural Geology*, **17**, 1741-1755.

KIM, Y.-S. 2000. *Damage structures and fault evolution around strike-slip faults*. Unpublished PhD. thesis, University of Southampton.

KIM, Y.-S., ANDREWS, J.R. and SANDERSON, D.J. 2000. Damage zones around strike-slip fault systems and strike-slip fault evolution, Crackington Haven, southwest England. *Geoscience Journal,* **4**, 53-72.

KIM, Y.–S., PEACOCK, D.C.P., SANDERSON, D.J. (in press). Strike-slip faults and damage zones at Marsalforn, Gozo Island, Malta. *Journal of Structural Geology.*

LARSEN, P.H. 1988. Relay structures in a Lower Permian basement-involved extensional system, East Greenland. *Journal of Structural Geology*, **10**, 3-8.

LAWN, B. 1993. *Fracture of Brittle Solids*, 2nd edition. Cambridge University Press, New York.

LEVERIDGE B.E., HOLDER, M.T., GOODE, A.J.J., SCRIVENER, R.C., JONES, N. & MERRIMAN, R.J. *in press. Geology of the Plymouth and south-east Cornwall district*. Memoir of the Geological Survey, sheet 348 (England and Wales).

LOGAN, J.M., FRIEDMAN, M., HIGGS, N., DENGO, C. and SHIMAMOTO, T. 1979. Experimental studies of simulated gouge and their application to studies of natural fault zones. *United States Geological Survey Open-File Report,* **79-1239**, 305-343.

MCKINSTRY, H.E. 1953. Shears of the second order. *American Journal of Science*, **251**, 401-414.

MOORE, D.E. and LOCKNER, D.A. 1995. The role of microcracking in shear-fracture propagation in granite. *Journal of Structural Geology,* **17**, 95-114.

NEMAT-NASSER, S. and HORII, H. 1982. Compression-induced nonplanar crack extension with application to splitting, exfoliation, and rockburst. *Journal of Geophysical Research*, **87**, 6805-6821.

NICOL, A., WATTERSON, J., WALSH, J.J. and CHILDS, C. 1996. The shapes, major axis orientations and displacement patterns of fault surfaces. *Journal of Structural Geology,* **18,** 235-248.

PEACOCK, D.C.P. 1991. Displacement and segment linkage in strike-slip fault zones. *Journal of Structural Geology,* **13**, 1025-1035.

PEACOCK, D.C.P. and SANDERSON, D.J. 1991. Displacement and segment linkage and relay ramps in normal fault zones. *Journal of Structural Geology,* **13**, 721-733.

PEACOCK, D.C.P. and SANDERSON, D. J. 1995. Strike-slip relay ramps. *Journal of Structural Geology,* **17**, 1351-1360.

PEACOCK, D.C.P. and SANDERSON, D.J. 1996. Effects of propagation rate on displacement variations along faults. *Journal of Structural Geology,* **18**, 311-320.

PETIT, J.-P. and BARQUINS, M. 1988. Can natural faults propagate under Mode II conditions? *Tectonics,* **7**, 1243-1256.

RAMSAY, J.G. and HUBER, M.I. 1987. *The Techniques of Modern Structural Geology.* Volume 2, Folds and fractures. Academic Press, London.

SEGALL, P. and POLLARD, D.D. 1983. Nucleation and growth of strike-slip faults in granite. *Journal of Geophysical Research,* **88**, 555-568.

SIBSON, R.H. 1989. Earthquake faulting as a structural process. *Journal of Structural Geology,* **11**, 1-14.

SWANSON, M.T. 1988. Pseudotachylyte-bearing strike-slip duplex structures in the Fort Foster Brittle Zone, S. Maine. *Journal of Structural Geology,* **10**, 813-828.

SWANSON, M.T. 1989. Sidewall ripouts in strike-slip faults. *Journal of Structural Geology,* **11**, 933-948.

TCHALENKO, J.S. 1970. Similarities between shear zones of different magnitudes. *Geological Society of America Bulletin*, **81**, 1625-1640.

THOMAS, A.L. and POLLARD, D.D. 1993. The geometry of echelon fractures in rock: Implications from laboratory and numerical experiments. *Journal of Structural Geology*, **15**, 323-334.

TRUDGILL, B.D. and CARTWRIGHT, J.A. 1994. Relay ramp forms and normal fault linkages - Canyonlands National Park, Utah. *Bulletin of the Geological Society of America*, **106**, 1143-1157.

VERMILYE, J.M. and SCHOLZ, C.H. 1999. Fault propagation and segmentation: insight from the microstructural examination of a small fault. *Journal of Structural Geology*, **21**, 1623-1636.

WALSH, J.J. and WATTERSON, J. 1990. New methods of fault projection for coalmine planning. *Proceedings of the Yorkshire Geological Society,* **48**, 209-219.

WALSH, J.J. and WATTERSON, J. 1991. Geometric and kinematic coherence and scale effects in normal fault systems. In: ROBERTS, A.M., YIELDING, G. and FREEMAN, B. (eds), *The geometry of normal faults*. Geological Society, London, Special Publication, **56**, 193-203.

WALSH, J.J., WATTERSON, J., BAILEY, W.R. and CHILDS, C. 1999. Fault relays, bends and branch-lines. *Journal of Structural Geology,* **21**, 1019-1026.

WERNICKE, B. 1981. Low-angle normal faults in the Basin and Range Province: nappe tectonics in an extending orogen. *Nature,* **291**, 645-648.

WILLEMSE, E.J.M., POLLARD, D.D. and AYDIN, A. 1996. Three-dimensional analyses of slip distributions on normal fault arrays with consequences for fault scaling. *Journal of Structural Geology*, **18**, 295-309.

WOODCOCK, N.H. and FISCHER, M. 1986. Strike-slip duplexes. *Journal of Structural Geology*, **8**, 725-735.